Empirical model description of photon path length for differential path length spectroscopy: combined effect of scattering and absorption

Stephen C. Kanick
Henricus J. C. M. Sterenborg
Arjen Amelink
Erasmus Medical Center
Department of Radiation Oncology
Center for Optical Diagnostics and Therapy
P.O. Box 2040
3000 CA Rotterdam, The Netherlands

Abstract. Differential path length spectroscopy (DPS) is a method of reflectance spectroscopy that utilizes a specialized fiber geometry to make the photon path length (τ) insensitive to variations in tissue optical properties over a wide range of absorption (μ_a) and total scattering (μ_s) coefficients, which are common within the ultraviolet/visible (UV/VIS) wavelength region. This study extends the description of τ to larger μ_a and smaller μ_s values, optical properties that are representative of the near-infrared region (NIR), a region where the DPS path length may be dependent on both coefficients. This study presents a novel empirical relationship between τ and the combined effect of both μ_a (range: 0.1–12 mm^{-1}) and μ_s (range: 1.5–42 mm^{-1}), anisotropy of 0.8, and is applicable to DPS probes containing a wide range of fiber diameters (range: 100–1000 μm). The results indicate that the simple empirical formula, including only one fitted parameter, is capable of accurately predicting τ over a wide range (r=0.985; range: 80–940 μm) and predictions are not biased versus μ_a or μ_s. This novel relationship is applicable to analysis of DPS measurements of tissue in both the UV/VIS and NIR wavelength regions and may provide information about the wavelength-specific tissue volume optically sampled during measurement. [DOI: 10.1117/1.3050424]

Keywords: Biomedical optics; reflectance; spectroscopy.

Paper 08352R received Oct. 2, 2008; revised manuscript received Nov. 6, 2008; accepted for publication Nov. 7, 2008; published online Dec. 23, 2008.

1 Introduction

Diffuse reflectance measurements of tissue are complicated by the effect that tissue optical properties have on the photon path length.[1–3] As photons propagate through tissue, they undergo scattering and absorption events, with the likelihood of these interactions given by the total scattering and absorption coefficients (μ_s and μ_a, respectively). [1,2] Classical diffuse reflectance devices collect photons with path lengths that are heavily dependent on the μ_s and μ_a values within the tissue being optically sampled.[2,3] This complicates spectral analysis, because the Beer–Lambert law requires accurate knowledge of the photon path length in order to estimate chromophore concentrations within the optically sampled tissue volume.[3] Moreover, the dependence of path length on optical properties has an effect on the tissue volume sampled during measurement, with measurements of different tissues potentially interrogating different volumes, or measurements of multiple wavelengths on the same tissue sample interrogating different volumes at different wavelengths, due to the wavelength-specific optical properties.

Our group has previously developed differential path length spectroscopy (DPS), which utilizes a unique fiber geometry to selectively sample photons that have propagated shallow depths into the tissue, making the path length approximately equal to the fiber diameter.[4] This fiber geometry allows accurate control of the path length and overcomes the classical limitation of unknown photon path length during diffuse reflectance measurements. The DPS path length, τ, is insensitive to variations in both μ_s and μ_a over a wide range of values commonly experienced in the ultraviolet/visible (UV/VIS) wavelength region, a phenomenon that has been investigated by both Monte Carlo modeling[4] and experimental measurement.[5] In the latter study,[5] it was noted that relatively large μ_a values for the UV/VIS region ($\mu_a > 1$ mm^{-1}) caused a reduction in the DPS path length. These absorption values could be observed in highly vascularized tissue due to strong absorption bands of hemoglobin in the 300–600 nm wavelength region. Therefore, the relationship was described by an empirical formula relating the dimensionless DPS path length (τ / d_{fiber}) to the dimensionless absorption coefficient, given as the product $\mu_a d_{fiber}$. This formula held for a wide range of μ_a values (range: 0.1–6.4 mm^{-1}) and fiber diameters (range: 200–1000 μm). The same study[5] also reported that very

Address all correspondence to Stephen Chad Kanick, Erasmus Medical Center, Center for Optical Diagnostics and Therapy, Department of Radiation Oncology, P.O. Box 2040, 3000 CA Rotterdam, The Netherlands. Tel.: +31-10-7032102; E-mail: s.kanick@erasmusmc.nl

1083-3668/2008/13(6)/064042/8/$25.00 © 2008 SPIE

small μ_s values for the UV/VIS region ($\mu_s < 5\ mm^{-1}$) increased the DPS path length, an effect that was not modeled because such small scattering values are not commonly experienced in the UV/VIS range. These results indicated that the DPS path length could be accurately estimated during analysis of tissue spectra in the UV/VIS region.

However, the findings indicated that the current description of DPS path length was not directly extensible to the near-infrared (NIR) wavelength region. This is because the NIR region contains larger μ_a ($\approx 10\ mm^{-1}$) and smaller μ_s ($\approx 2\ mm^{-1}$) values than the UV/VIS region,[6–8] potentially making the NIR-DPS path length more dependent on the absolute value of these coefficients. This study reports DPS path lengths measured in optical phantoms that contain variations in the combinations of μ_s and μ_a values that are representative of the NIR wavelength region. The measurements are made with DPS probe fiber diameters of 100 and 200 μm, small fibers specifically selected to collect appreciable amounts of light from measurements of a medium containing large absorption coefficients. Additionally, this study utilizes previously reported data[5] that showed the effect of independent variations in μ_s and μ_a on the DPS path length for fiber diameters of 200–1000 μm. The data are utilized to develop a novel empirical formula that describes the combined effect of both absorption and scattering on the DPS path length for a wide range of optical properties representative of the NIR wavelength region in tissue.

2 Methods

2.1 *DPS*

DPS utilizes a specialized fiber geometry to selectively sample superficial layers of tissue with a known photon path length. The DPS probe contains two fibers: one used for delivery and collection (dc) and an adjacent fiber used for collection (c). During measurement, photons exit the dc fiber, scatter throughout the tissue, and are collected by both the dc and c fibers. The dc fiber collects photons that have scattered a range of different distances throughout the tissue, a subset of which has traveled short distances before being backscattered by the superficial layers of tissue. Comparatively, the c fiber signal collects approximately the same number of deeply scattered photons, but this probe does not contain a subset of superficially backscattered photons. The difference between the signals collected by the dc and c fiber contains the contribution from photons that interrogated shallow tissue depths. This relationship can be expressed as follows:

$$\mathbf{R} = \mathbf{I} - \mathbf{J}, \tag{1}$$

where $\mathbf{I}$ is the light intensity collected by the dc fiber, $\mathbf{J}$ is the light intensity collected by the c fiber, and $\mathbf{R}$ is the differential reflectance. All symbols marked in boldface type are considered wavelength dependent. Attenuation of the $\mathbf{R}$ signal by addition of a chromophore can be described using the Beer–Lambert law as follows:

$$\mathbf{R} = \mathbf{R_o} \exp(-\boldsymbol{\mu}_\mathbf{a}^\mathbf{i} C_i \boldsymbol{\tau}), \tag{2}$$

where $\mathbf{R_o}$ is the differential reflectance prior to addition of the chromophore, $\boldsymbol{\mu}_\mathbf{a}^\mathbf{i}$ and C_i are the specific absorption coefficient and concentration of the chromophore i, respectively, and $\boldsymbol{\tau}$ is the mean path length of photons contributing to the differential signal, $\mathbf{R}$.

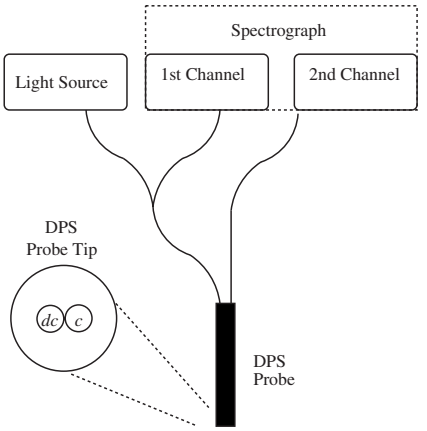

Fig. 1 Schematic of DPS probe. The probe tip shows both the delivery and collection fiber (dc) and the adjacent collection fiber (c).

3 DPS Instrumentation

Figure 1 shows a schematic of the DPS setup used to measure optical phantoms in this study. The device contains a spectrophotometer (SD 2000; Ocean Optics; Duiven, The Netherlands) and halogen light source (HL-2000-FHSA; Ocean Optics; Duiven, The Netherlands). During measurement, photons travel from the light source through one arm of a bifurcated fiber and through the dc fiber, after which it exits into the sample. Reflected photons that are collected by the dc fiber travel through the second arm of the bifurcated fiber and into the first channel of the spectrophotometer. Reflected photons that are collected by the c fiber travel directly into the second channel of the spectrophotometer. Spectral reflections at the probe tip due to refractive index mismatch between the fiber and sample are minimized by polishing the DPS probe tip at an angle of 15 deg.[9] A calibration procedure, described in detail elsewhere,[9] was utilized to account for other internal reflections, variability in lamp-specific output, and in fiber-specific transmission properties. The calibration involves measurement of both white and black Spectralon standards (Labsphere SRS-99 and SRS-02) in air and measurement of water within a dark container. These measurements are used to calculate the differential reflectance signal, $\mathbf{R}$, as

$$\mathbf{R} = c_{cal}\left[\frac{(\mathbf{I} - \mathbf{I}_{water})}{(\mathbf{I}_{white} - \mathbf{I}_{black})} - \frac{\mathbf{J}}{(\mathbf{J}_{white} - \mathbf{J}_{black})}\right]. \tag{3}$$

Here, the measured intensity ($\mathbf{I}$) is reduced by the intensity attributable to internal reflections ($\mathbf{I}_{water}$). Both the $\mathbf{I}$ and $\mathbf{J}$ signals are normalized by the difference between intensities measured from white and black spectralons, and the calibration constant, c_{cal}, accounts for the specific distance between the fiber probe tip and spectralon surface during calibration measurements.

3.1 *Optical Phantom Preparation*

Optical phantoms were prepared by mixing Intralipid 20% (Fresenius Kabi AG, Bad Homburg, Germany), Evans Blue powder (Sigma-Aldrich, Inc., Vienna, Austria), and saline solution (0.9%). The μ_a of each phantom was selected by varying the concentration of Evans Blue, which has an absorption (μ_a^{EB}) maximum of 18 L/(g mm) at 611 nm. The μ_s of each phantom was selected by varying the amount of Intralipid 20%, which has a μ_s of 80 mm^{-1} and an anisotropy of $g \approx 0.8$ when undiluted at 611 nm. Because Intralipid is not an optical standard, the optical properties of the batch utilized in this study were verified using a spatially resolved diffuse reflectance measurement, as has been done previously.[10]

Phantoms were constructed with scattering coefficients of $\mu_s = 1.5$, 3, 6, 9, 12, 20, and 42 mm^{-1}, for each absorption coefficient of: $\mu_a = 0.4$, 1, 3, and 12 mm^{-1}, representing 28 combinations of optical properties. Also, additional phantoms were prepared at each selected μ_s with no Evans Blue added, which were utilized to obtain baseline measurements of $\mathbf{R_o}$ that represented $\mu_a = 0$ mm^{-1} at 611 nm. Each phantom consisted of a 10-mL sample contained within a 24-mm-diameter cylindrical container. Phantoms for each paired value of optical properties were independently prepared three times and measured by DPS probes with d_{fiber} of 100 and 200 μm.

This study also incorporated DPS path length data reported previously.[5] Phantoms in that previous study were constructed in the same manner as described here. Those data included variations in the absorption coefficient $\mu_a = 0.1$, 0.2, 0.4, 0.8, 1.6, 3.2, and 6.4 mm^{-1} for a constant scattering coefficient $\mu_s = 15$ mm^{-1}, and also variations in the scattering coefficient $\mu_s = 1.5$, 3, 6, 9, 12, 15, 23, and 42 mm^{-1} for a constant absorption coefficient of $\mu_a = 0.4$ mm^{-1}. These phantoms were measured with DPS probes containing fiber diameters of $d_{fiber} = 200$, 400, 600, 800, and 1000 μm.

During measurement by DPS, the probe was lowered into the phantom so that the probe tip was below the meniscus of the phantom surface. Boundary effects were assumed to be negligible after measurement of 10 mL phantoms was not shown to be different than 40-mL phantoms. During the measurement of each phantom, the DPS recorded 10 sequential measurements on each phantom with the integration time adjusted to obtain adequate collected light intensity from measurement of each phantom.

3.2 *Data Analysis*

The Beer–Lambert law was used to describe attenuation of the DPS reflectance signal, $\mathbf{R}$, due to the addition of an absorber, as in Eq. (2). Basis reflectance measurements of $\mathbf{R_o}$ were made on phantoms prepared for each scattering coefficient with no Evans Blue added, and measurements of $\mathbf{R}$ were made on phantoms prepared with the same scattering coefficient plus the addition of Evans Blue. Changes between $\mathbf{R}$ and $\mathbf{R_o}$ were assumed to be attributable to the difference in absorption coefficient between the two samples. Therefore, the difference between $\mathbf{R}$ and $\mathbf{R_o}$ was measured at a wavelength where the optical properties were known (at 611 nm). This was calculated by normalizing $\mathbf{R_o}$ and $\mathbf{R}$ over the wavelength range 750–800 nm (to account for small vertical shifts in the collected light intensities). This normalization procedure accounts for small differences in fiber transmission due to differences in fiber bending for the paired phantom measurements. Typically, these transmission differences are less than 1%, but for small absorption coefficients, such small differences would have a large effect on the calculated path lengths. The DPS path length was calculated at 611 nm as

$$\tau = \frac{-\ln(R/R_o)}{(\mu_a^{EB} C_{EB})}. \tag{4}$$

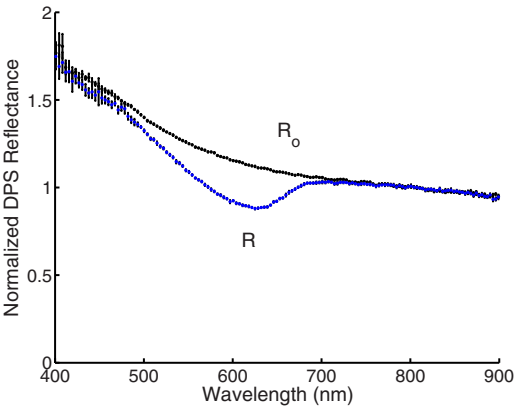

Fig. 2 DPS reflectance spectra measured from Intralipid 20% solution ($\mu_s = 42$ mm^{-1}) both with Evans Blue added ($\mathbf{R}$, $\mu_a = 1$ mm^{-1} at 611 nm) and without ($\mathbf{R_o}$). Spectra are normalized to the mean reflectance value over the wavelength range 750–800 nm.

3.3 *Empirical Model of DPS Path Length*

Observations of the effect of variations in μ_s and μ_a on the DPS path length led to the selection of the following model:

$$\frac{\tau_{model}}{d_{fiber}} = \frac{(1 + (\mu_s d_{fiber})^{-a})}{(1 + (\mu_a d_{fiber})^{a})}. \tag{5}$$

Here, a is a parameter fitted by minimizing the residual error between measured and predicted dimensionless path length (τ / d_{fiber}), with each point weighted by the inverse of the standard error of the mean (SEM), calculated as SEM = standard deviation/square root of the number of data points. Confidence intervals on parameter estimates were calculated from the square root of the diagonal of the covariance matrix, a technique that is described in detail elsewhere.[11] Parameter estimation was achieved using a Levenberg–Marquardt algorithm[12] that was scripted into LabView code (vers. 7.1.1, National Instruments).

4 Results

4.1 *DPS Reflectance Data*

DPS reflectance spectra were measured at a resolution of 2048 pixels over the wavelength range 340–1027 nm. The data were smoothed by averaging data into bins of 10 pixels, which allowed the calculation of a standard deviation that represents noise within the signal.[5] Figure 2 shows the normalized DPS reflectance intensity data over the range 400–900 nm from measurements with $d_{fiber} = 200$ μm on op-

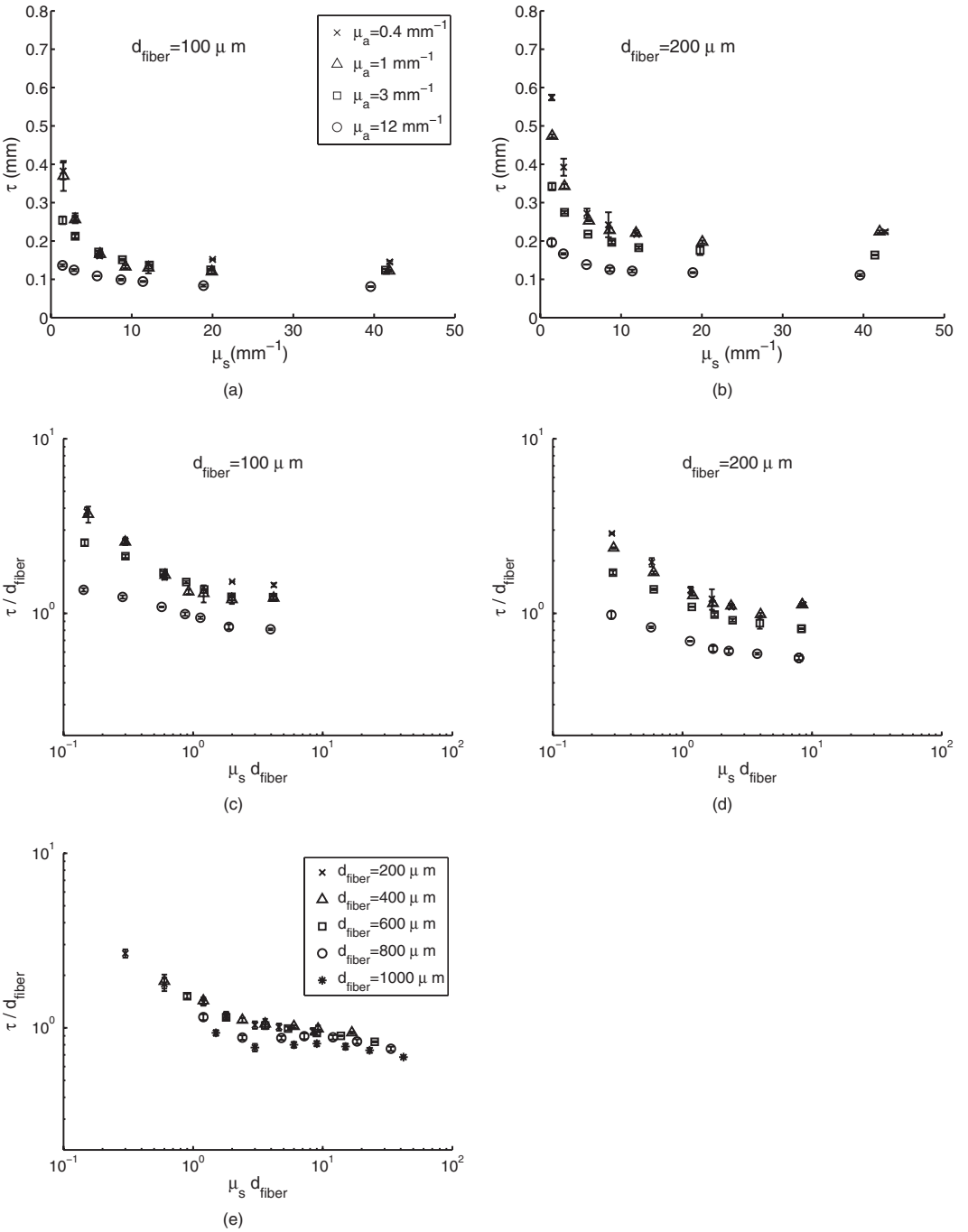

Fig. 3 (a) and (b) show the effect of μ_s on DPS path length for selected μ_a values, as measured by DPS fiber diameters of 100 and 200 μm, respectively. (c) and (d) show the effect of dimensionless scattering $\mu_s d_{fiber}$ on dimensionless DPS path length (τ/d_{fiber}) for DPS fiber diameters of 100 and 200 μm, while (e) shows the same relationship for constant μ_a (0.4 mm^{-1}) measured over a range of DPS probe diameters (200–1000 μm).

tical phantoms without Evans Blue, $\mathbf{R_o}$ (μ_s=42 mm^{-1} and μ_a=0 mm^{-1}), and with Evans Blue, $\mathbf{R}$ (μ_s=42 mm^{-1} and μ_a=1 mm^{-1}).

4.2 *DPS Path Length Dependence on μ_s*

Figures 3(a) and 3(b) show the DPS path length, extracted from the measurement using Eq. (4), versus μ_s for various selected values of μ_a as measured by DPS probes with fiber diameters of 100 and 200 μm, respectively. Here, data points represent the mean from DPS measurements of three independent optical phantoms, and the error bars indicate one standard deviation about the mean. Inspection of the data show two regimes: (*i*) τ is sensitive to scattering changes for relatively small μ_s, and (*ii*) τ is insensitive to changes over a range of larger μ_s. In order to properly compare the effect of μ_s on τ over a range of fiber diameters, it is important to consider the relationship between dimensionless DPS path length (τ/d_{fiber}) and dimensionless scattering ($\mu_s d_{fiber}$). These

relationships are shown on log–log scale for the 100 and 200 μm data in Figs. 3(c) and 3(d), respectively. Additionally, Fig. 3(e) shows (τ/d_{fiber}) versus $(\mu_s d_{\text{fiber}})$ for measurements of optical phantoms with constant $\mu_a=0.4$ mm^{-1}, as measured by DPS probes with d_{fiber} over the range 200–1000 μm. The dimensionless data show that the transition of the DPS path length from sensitive to insensitive occurs at $(\mu_s d_{\text{fiber}} < \approx 2)$. This transition region is also observable for the d_{fiber} of 100 and 200 μm probes on Figs. 3(c) and 3(d), with the trend affected by the magnitude of μ_a. It is worth noting that the effect of scattering on DPS path length was investigated by varying μ_s while holding μ_a constant, however, the path length is dependent on dimensionless absorption. Therefore, dimensionless path lengths for a constant μ_a that are measured with different d_{fiber} values do not uniformly collapse onto one another; instead, the larger fiber diameters will have a more pronounced effect from absorption. This phenomenon accounts for differences in the dimensionless path lengths as measured by 100 and 200 μm [visible in Figs. 3(c) and 3(d)]. This effect is also evident in Fig. 3(e), where the dimensionless path for larger DPS fiber diameters of 800 and 1000 μm deviate from the rest of the group.

4.3 *DPS Path Length Dependence on μ_a*

Figures 4(a) and 4(b) show the DPS path length versus μ_a for various selected values of μ_s, as measured by DPS probes with d_{fiber} of 100 and 200 μm, respectively. Again, data points represent the mean from DPS measurements of three independent optical phantoms, and the error bars indicate one standard deviation about the mean. The data show an expected trend, with an increase in μ_a causing a reduction in τ. Here, comparison of data over multiple fiber diameters is aided by visualizing τ/d_{fiber} versus the dimensionless absorption $\mu_a d_{\text{fiber}}$. These data are shown on log–log scale for the 100 and 200 μm data in Figs. 4(c) and 4(d), respectively. These data show a general reduction in dimensionless DPS path length as dimensionless absorption increases, with vertical stratification of the dimensionless path lengths at constant values of dimensionless scattering. Figure 4(e) shows (τ/d_{fiber}) versus $(\mu_a d_{\text{fiber}})$ for measurements of optical phantoms with constant $\mu_s=15$ mm^{-1}, as measured by DPS probes with d_{fiber} over the range 200–1000 μm. The data presented in plot Fig. 4(e) were reported in our previous study,[5] and these data were used to model the previously published relationship between τ and μ_a. The data show a small effect of μ_a variation on τ for small dimensionless absorption coefficients, with more pronounced effects when for $\mu_a d_{\text{fiber}} > 0.6$.

4.4 *Empirical Model of DPS Photon Path Length as a Function of μ_s and μ_a*

Figure 5(a) shows τ_{model}, the DPS path length predicted by Eq. (5), versus τ, the DPS path length measured empirically. The estimated parameter value of $a=0.53\pm0.09$ resulted in the smallest weighted residual error between data and model predictions. Model predictions were significantly correlated with measured values, as evidenced by a Pearson product correlation coefficient of $r=0.985$; this effect is observable in the plot as the data are scattered about the line of unity. Figure 5(b) plots the data on a log–log scale, which shows that the relationship holds for small path lengths. In order to observe the quality of model predictions over a wide range of DPS path lengths (range: 80–940 μm), Fig. 5(c) shows the residual error as a fraction of the measured DPS path length value [residual percentage$=100\times(\tau-\tau_{\text{model}})/\tau$], versus the measured τ values, with error bars calculated as the ratio of the standard deviation to the mean, representing the uncertainty in each measured data point. This plot shows the residual error scattered about zero across the range of DPS path lengths. The mean absolute residual error percentage is $8.5\pm6.9\%$. Here, 97% of the data points have an absolute residual error that is $\leqslant 20\%$ within the measurement error. The remaining 3% of the data points are characterized by extreme optical properties: large μ_a, small μ_s, small d_{fiber}.

Additionally, the residuals displayed on Fig. 5(c) were not correlated with either $\mu_s d_{\text{fiber}}$ or $\mu_a d_{\text{fiber}}$, with Pearson product correlation coefficients of $r=-0.170$ and -0.028, respectively. This indicates that the model predictions are not biased as a function of either dimensionless scattering or dimensionless absorption, which confirms that the selected model structure is appropriate and that incorporation of additional fitted parameters would only describe noise within the data.

5 Discussion and Conclusions

The DPS device utilizes a specific fiber geometry to make the photon path length insensitive to changes in the tissue optical properties and instead dependent on the fiber diameter. Previously reported data support this claim for ranges of optical properties common within the UV/VIS wavelength region.[4,5] However, this assumption is not suitable for the large absorption and small scattering coefficients that are common within the NIR wavelength region.[7,8] This study presents a novel empirical formula that describes the dependence of the DPS photon path length on both total scattering and absorption coefficients over the range of values experienced within the NIR wavelength region. This relationship is valid for a wide range of μ_s (range: 1.5–42 mm^{-1}) and μ_a (range: 0.1–12 mm^{-1}) values and for a wide range of DPS fiber diameters (100–1000 μm). This formula allows analysis of DPS spectra from tissue containing a wider range of biological measurements than previously possible, including those properties common to the NIR wavelength range.

The empirical model presented in Eq. (5) describes an intuitive relationship between the DPS path length and both μ_a and μ_s. As noted previously, the DPS path length is approximately equal to the fiber diameter for tissue measurements over a range of optical properties commonly experienced in the UV-VIS wavelength region. However, it has been shown that small μ_s values result in a DPS path length that is greater than the fiber diameter. This phenomenon is captured by the numerator of Eq. (5), where for large μ_s values the numerator $[1+(\mu_s d_{\text{fiber}})^{-a}]$ approaches 1, resulting in a DPS path length that approximates the fiber diameter; while for small μ_s values, the numerator becomes >1, resulting in an increased DPS path length. Conversely, large μ_a values result in a decreased DPS path length. This phenomenon is captured by the denominator of Eq. (5), where for small μ_a values, the denominator $[1+(\mu_a d_{\text{fiber}})^{a}]$ approaches 1, resulting in a DPS path length that approximates the fiber diameter, while for large μ_a values, the numerator becomes <1, resulting in a

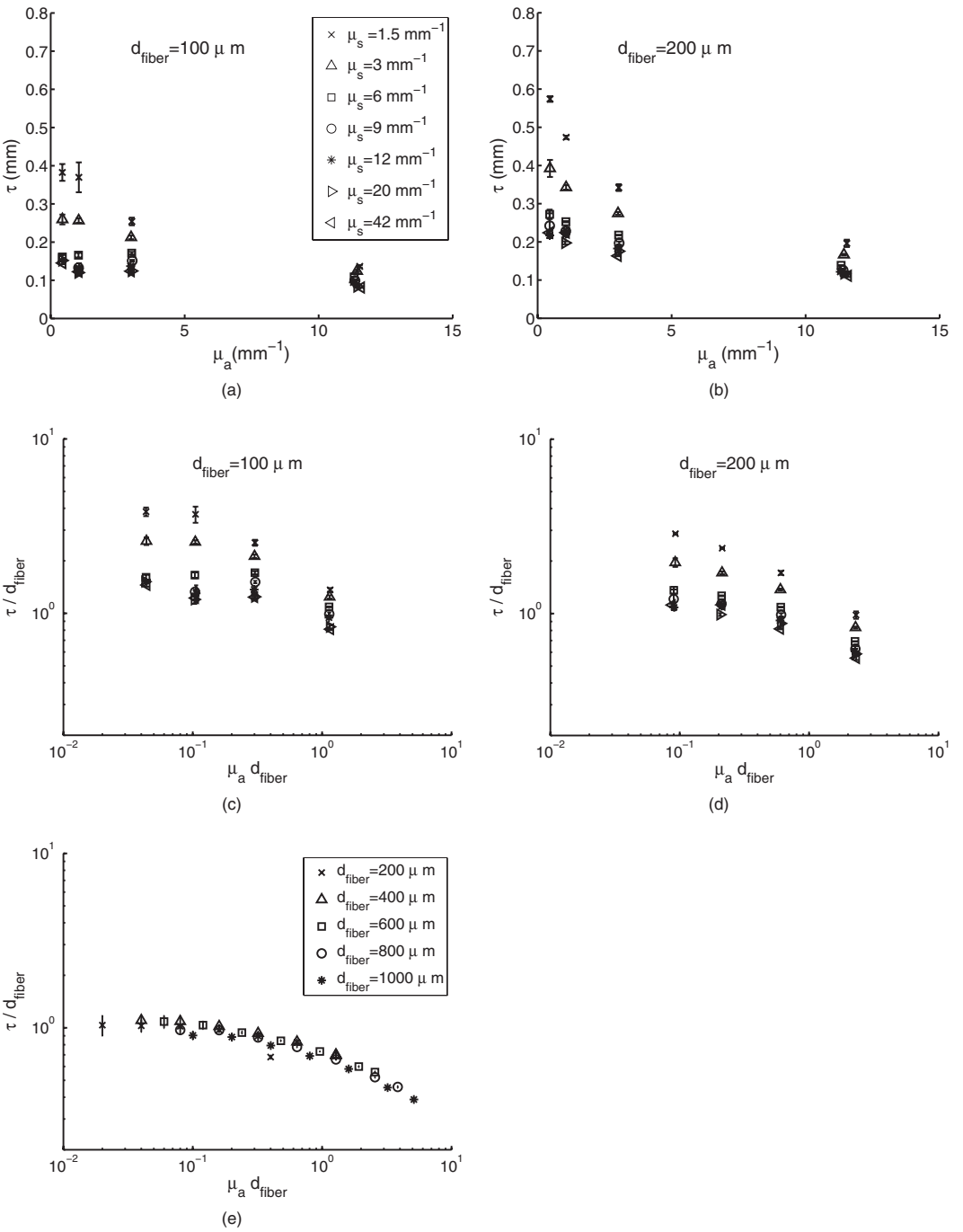

Fig. 4 (a) and (b) show the effect of μ_a on DPS path length for selected μ_s values, as measured by DPS fiber diameters of 100 and 200 μm, respectively. (c) and (d) show the effect of dimensionless absorption $\mu_a d_{fiber}$ on dimensionless DPS path length (τ/d_{fiber}) for DPS fiber diameters of 100 and 200 μm, while (e) shows the same relationship for constant μ_s (15 mm^{-1}) measured over a range of DPS probe diameters (200–1000 μm).

reduced DPS path length. The resulting model structure is capable of capturing the effects of both μ_s and μ_a with only one fitted parameter.

The results presented in this paper suggest that the empirical model presented in Eq. (5) is able to accurately describe the effect of variations in both μ_s and μ_a. This conclusion is based on the high correlation between measured and predicted DPS path lengths (r=0.985), the observation that the residuals are scattered about zero [with no observable trends, as shown in Fig. 5(c)], and the lack of correlation of residuals with either μ_s or μ_a. Moreover, the mean absolute residual error of 8.4% appears reasonable when considering that the model contains only one fitted parameter and that the model was fitted to data values that spanned very large ranges: a 120-fold change in μ_a, a 28-fold change in μ_s, and a 10-fold change in d_{fiber}. Therefore, the authors expect that the error associated with the experimental construction and measure-

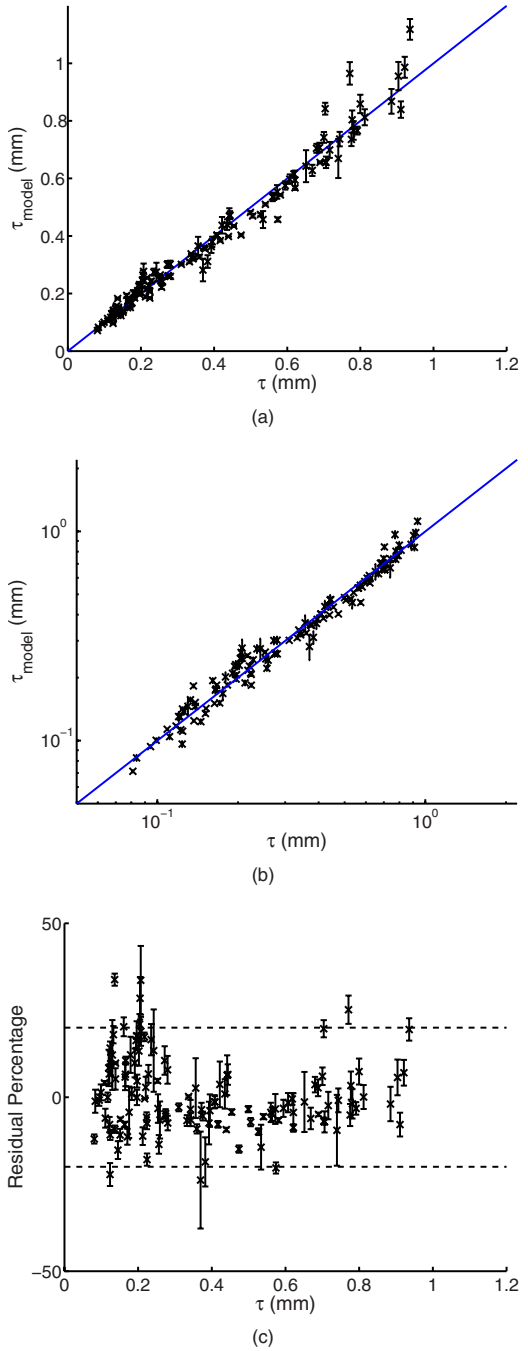

Fig. 5 Measured versus model predicted DPS path length on a linear (a) and log (b) scale, with the line of unity included for comparative purposes. (c) Residual plot showing percentage deviation of model prediction from measured DPS path length versus measured value, with ±20% indicated with dashed lines.

ment of the optical phantoms may be equivalent to any inadequacy within the model.

The work presented here is a logical extension of our previous study, which quantified the effect that independent variation of either μ_s or μ_a had on the DPS path length.[5] In that previous study[5] it was reported that the DPS path length is insensitive to changes in scattering coefficient over a broad range, with the path length varying only 16% over the range $5\ \text{mm}^{-1} < \mu_s < 50\ \text{mm}^{-1}$ for fiber diameters in the range 400–1000 μm. The change was more pronounced for the fiber diameter of 200 μm, which had 25% variation, and it was hypothesized that this effect would be magnified for a DPS fiber diameter of 100 μm. This study investigated and confirmed that hypothesis, finding 38% variation for the 100 μm over the same μ_s range. Moreover, this study incorporated the effect that changes in μ_s have on the DPS path length, which were shown to be appreciable for $\mu_s d_{\text{fiber}} < 2$. This study develops the correlation between DPS path length and μ_s for a constant anisotropy value of $g \approx 0.8$, and the effect of anisotropy variation over the range of values expected within tissue in both the UV-VIS and NIR wavelength regions (range: $g \approx 0.7$–0.95) on the DPS path length is not well-characterized. The authors expect anisotropy to have a more pronounced effect on the DPS path length for samples with small μ_s and for measurements with small fiber diameters. In these situations, collected photons have undergone relatively few scattering events and therefore, the direction of individual scattering events is expected to have a more pronounced effect on the mean DPS photon path length.

Also in the previous study,[5] changes in absorption coefficient over the range $0\ \text{mm}^{-1} < \mu_a < 1\ \text{mm}^{-1}$ caused only a 15% variation in the DPS path length. This effect increased for increasing μ_a, and while the DPS path length was insensitive to μ_a for $\mu_a d_{\text{fiber}} < 0.6$, the effect was appreciable for $\mu_a d_{\text{fiber}} > 0.6$. An empirical formula was utilized to describe the relationship over a wide range of absorption values (range $\mu_a = 0.1$–$6.4\ \text{mm}^{-1}$), specifically, the model was utilized to describe the data presented in Fig. 4(e). Comparing the predictions from that previous model with the model presented in Eq. (5), the predictions are nearly identical for estimation of the original data set (with a Pearson correlation coefficient of $r = 0.990$). This indicates that the novel formula presented in this study is capable of capturing the previously modeled effect with the same accuracy, with the enhanced aspect of incorporating scattering effects on the path length. The tissue μ_s in the UV-VIS region is typically in the range 5–50 mm^{-1}, and recalculation of the data presented in Fig. 4(e) (originally calculated with $\mu_s = 15\ \text{mm}^{-1}$) for a μ_s of either 5 or 50 mm^{-1} results in a change to the model predicted path length of $\leqslant 20\%$, for either case. This source of error is similar to that introduced by the assumption of insensitivity of the DPS path length to physiologically relevant changes in scattering, as required by the model presented by Kaspers et al.[5] These results indicate that the novel formula has potential application for analysis of DPS tissue spectra measured in both the UV/VIS and NIR wavelength regions.

It is important to consider the assumptions required to incorporate the novel pathlength formula into a spectral analysis algorithm. Previously, the algorithm used to analyze DPS spectra was able to capture the effects of scattering on the reflectance by specifying a background scattering model (such as Mie scattering,[13,14] or a combination of Mie and Rayleigh scattering.)[11,15] The analysis included the assumption that the DPS path length was independent of the total scattering coefficient. Therefore, no estimation of an absolute value for μ_s was required (which was valid for measurements in the UV/VIS range). However, the formula for DPS path length presented in this study [in Eq. (5)] is dependent on the absolute

μ_s value, necessitating the estimation (or calculation) of μ_s, an assumption that may have a pronounced effect on DPS path length in the NIR wavelength region. This may be addressed by specifying the scattering model (as before) and simply assuming an absolute value of μ_s at one wavelength, allowing the algorithm to describe wavelength-dependent changes within the spectra; however, this may be a source of error in the analysis, because the absolute value of μ_s may not be known with high certainty. Hypothetically, this limitation could be addressed through a calibration procedure that would allow accurate estimation of the total scattering coefficient; this is an area of future work.

This novel description of DPS path length as a function of both absorption and total scattering coefficients may enhance analysis of clinical data. This relationship is required for analysis of DPS measurements in the NIR wavelength region, where the relative extreme optical properties (compared with the UV/VIS wavelength region) would affect the DPS path length and would otherwise introduce error into estimates of absorber concentrations within the tissue. This formula also allows estimation of a wavelength-specific DPS photon path length, which may provide information about the volume of tissue optically sampled during measurement, a factor that may vary between UV/VIS and NIR measurements on the same tissue. In a broader sense, the formula presented here may allow estimation of changes in the total scattering coefficient within tissue in response to a clinical procedure such as photodynamic therapy, or allow accurate estimation of differences in the total scattering coefficient between normal and diseased tissue, useful in tissue diagnostics.

Acknowledgments

The authors thank B. Kruijt and F. van Zaane for assistance in constructing the DPS fiber probes, and D. J. Robinson for helpful discussions. This research is supported by the Dutch Technology Foundation STW, Applied Science Division of NWO, and the Technology Program of the Ministry of Economic Affairs.

References

1. B. W. Wilson and S. L. Jacques, "Optical reflectance and transmittance of tissues: Principles and applications," *IEEE J. Quantum Electron.* **26**, 2186–2199 (1990).
2. D. T. Delpy and M. Cope, "Quantification in tissue near-infrared spectroscopy," *Philos. Trans. R. Soc. London* **352**, 649–659 (1997).
3. J. R. Mourant, I. J. Bigio, D. A. Jack, T. M. Johnson, and H. D. Miller, "Measuring absorption coefficients in small volumes of highly scattering media: Source-detector separations for which path lengths do not depend on scattering properties," *Appl. Opt.* **36**, 5655–5661 (1997).
4. A. Amelink and H. J. C. M. Sterenborg, "Measurement of the local optical properties of turbid media by differential path-length spectroscopy," *Appl. Opt.* **43**, 3048–3054 (2004).
5. O. P. Kaspers, H. J. C. M. Sterenborg, and A. Amelink, "Controlling the optical path length in turbid media using differential path-length spectroscopy: Fiber diameter dependence," *Appl. Opt.* **47**, 365–371 (2008).
6. W. Cheong, S. A. Prahl, and A. J. Welch, "A review of the optical properties of biological tissues," *IEEE J. Quantum Electron.* **26**, 2166–2185 (1990).
7. T. L. Troy and S. N. Thennadil, "Optical properties of human skin in the near infrared wavelength range of 1000 to 2200 nm," *J. Biomed. Opt.* **6**, 167–176 (2001).
8. E. Salomatina, B. Jiang, J. Novak, and A. N. Yaroslavsky, "Optical properties of normal and cancerous human skin in the visible and near-infrared spectral range," *J. Biomed. Opt.* **11**, 064026 (2006).
9. A. Amelink, M. P. L. Bard, S. A. Burgers, and H. J. C. M. Sterenborg, "Single-scattering spectroscopy for endoscopic analysis of particle size in superficial layers of turbid media," *Appl. Opt.* **42**, 4095–4101 (2003).
10. H. J. van Staveren, C. J. M. Moes, S. A. Prahl, and M. J. C. Vangemert, "Light-scattering in Intralipid-10-percent in the wavelength region of 400–1100 nm," *Appl. Opt.* **30**, 4507–4514 (1991).
11. A. Amelink, D. J. Robinson, and H. J. C. M. Sterenborg, "Confidence intervals on fit parameters derived from optical reflectance spectroscopy measurements," *J. Biomed. Opt.* **13**, 05040144 (2008).
12. D. Marquardt, "An algorithm for least-squares estimation of nonlinear parameters," *SIAM J. Appl. Math.* **11**, 431–444 (1963).
13. A. Amelink, A. van der Ploeg–van den Heuvel, W. J. de Wolf, D. J. Robinson, and H. J. C. M. Sterenborg, "Monitoring PDT by means of superficial reflectance spectroscopy," *J. Photochem. Photobiol., B* **79**, 243–251 (2005).
14. R. L. P. van Veen, A. Amelink, M. Menke-Pluymers, C. van der Pol, and H. J. C. M. Sterenborg, "Optical biopsy of breast tissue using differential path-length spectroscopy," *Phys. Med. Biol.* **50**, 2573–2581 (2005).
15. B. Kruijt, H. S. de Bruijn, A. van der Ploeg-van den Heuvel, R. W. de Bruin, H. J. Sterenborg, A. Amelink, and D. J. Robinson, "Monitoring ALA-induced PpIX photodynamic therapy in the rat esophagus using fluorescence and reflectance spectroscopy," *Photochem. Photobiol.* **84**, 1515–1527 (2008).